INTERNATIONAL JOURNAL OF CLIMATOLOGY
Int. J. Climatol. **37**: 4757–4767 (2017)
Published online 22 May 2017 in Wiley Online Library
(wileyonlinelibrary.com) DOI: 10.1002/joc.5119

RMetS
Royal Meteorological Society

Trends of land surface heat fluxes on the Tibetan Plateau from 2001 to 2012

Cunbo Han,[a,b,c†,*] Yaoming Ma,[a,b,c] Xuelong Chen[d] and Zhongbo Su[d]

[a] *Key Laboratory of Tibetan Environment Changes and Land Surface Processes, Institute of Tibetan Plateau Research, Chinese Academy of Sciences, CAS Center for Excellence in Tibetan Plateau Earth Sciences, Beijing, China*
[b] *Qomolangma Station for Atmospheric Environmental Observation and Research, Chinese Academy of Sciences, Dingri, Tibet, China*
[c] *University of Chinese Academy of Sciences, Beijing, China*
[d] *Faculty of Geo-Information Science and Earth Observation, University of Twente, Enschede, The Netherlands*

ABSTRACT: A parameterization approach of effective roughness length was introduced into the Surface Energy Balance System (SEBS) model to account for subgrid-scale topographical influences. Regional distribution of land surface heat flux values (including net radiation flux, ground heat flux, sensible heat flux, and latent heat flux) was estimated on the Tibetan Plateau (TP) based on the SEBS model, and utilizing remote sensing products and reanalysis datasets. We then investigated annual trends in these fluxes for the period 2001–2012. It was found that land surface net radiation flux increased slightly, especially in high, mountainous regions and the central TP, and was influenced by glacial retreat and topsoil wetting, respectively. Sensible heat flux decreased overall, especially in the central and northern TP. In the Yarlung Zangbo River (YZR) Basin, the sensible heat flux increased because of a rise in the ground-air temperature difference. The latent heat flux increased over the majority TP, except for areas in the YZR Basin. This can be attributed to increases in precipitation and vegetation greening.

KEY WORDS land surface heat flux trend; SEBS; effective roughness length; Tibetan Plateau

Received 8 July 2016; Revised 30 March 2017; Accepted 4 April 2017

1. Introduction

The Tibetan Plateau (TP) is the highest and largest plateau in the world. By acting as an elevated thermal source as well as a topographic barrier, the TP exerts a profound impact on both local weather and global climate (Ye and Gao, 1979; Yanai and Wu, 2006). In general, the view that this thermal source with strong sensible heating in the surface layer plays a crucial role in the onset and maintenance of the Asian summer monsoon (ASM) is accepted by most meteorologists (Yanai and Wu, 2006; Wu *et al.*, 2012, 2015). However, Boos and Kuang (2010) argued that it is the TPs topographical isolation, especially by the Himalaya Mountains on its southern periphery, and not the heating effect of the TP, i.e. the dominant control of the South Asian monsoonal system. Boos and Kuang (2013) have further showed that the South Asian monsoonal system is more sensitive to surface heat fluxes from nearby non-elevated surfaces than that to fluxes from the TP and from the slopes of Himalaya. They also pointed out that there is no available evidence to support the hypothesis that surface sensible heat flux values are any more influential than surface latent heat flux values. In contrast, Wu *et al.* (2012) argued that the thermal forcing from the TP instead provides the domain control for the monsoon system. Using a climate model, they showed that the monsoon strength decreased when the sensible heat fluxes from southern mountain ranges of the TP were suppressed. Furthermore, He *et al.* (2015) pointed out that it is the pumping of water vapour from sea and land due to the surface sensible heating of the TP and Iranian Plateaus that breeds the monsoon system from the astronomical and hydrological perspective. However, the estimation of surface sensible heat flux over the TP is always in dispute and still has big uncertainty. Thus, these findings have highlighted the necessity of investigating the land surface heat flux values on the TP as a possible heat source affecting the circulatory patterns of the South Asian monsoonal system.

The atmospheric heat source comprises three components, i.e. surface sensible heat flux, latent heat release to the atmosphere by condensation, and radiative convergence flux. Surface sensible heat flux is a major component of the heat source, and its investigation has been addressed extensively over the past several decades especially under rapid climate change on the TP (Yang *et al.*, 2011a). Growing evidence has shown that a striking change in the climate has occurred on the TP over the past half century (Yao *et al.*, 2012a; Yang *et al.*, 2014). The TP has, overall, experienced rapid surface air warming and moistening, solar dimming, and wind stilling since the beginning of the 1980s (Yang *et al.*, 2014). The solar dimming over the TP has been principally caused by the increase in water vapour

* Correspondence to: C. Han, Institute of Tibetan Plateau Research, Chinese Academy of Sciences, No. 16 Lincui Road, Chaoyang District, Beijing 100101, China. E-mail: hcb@itpcas.ac.cn; cunbo.han@hotmail.com

†Present address: Agrosphere Institute (IBG 3), Forschungszentrum Jülich GmbH, 52425 Jülich, Germany.

quantities and deep cloud cover (Yang *et al.*, 2012). These changes to the climate have led to the atmospheric heat source over the TP showing a significantly weakened trend (Yang *et al.*, 2011b). Studies have found that thermal forcing weakening over the TP was caused by a combination of enhanced cooling through radiation loss and a decrease in land surface sensible heat flux, especially in spring (Duan and Wu, 2008; Yang *et al.*, 2011a, 2011b; Zhu *et al.*, 2012). Recent field experiments on the TP have advanced our understanding of the climate change and heating processes on the TP (Ma *et al.*, 2008; Yao *et al.*, 2012b; Yang *et al.*, 2014). However, we still need to understand why and how surface heat flux values changed over the past decade, and how we can interpret any trends and spatial distribution patterns. There are a number of products of land surface heat flux values provided by numerical model simulation, such as Global Land Data Assimilation System (GLDAS), National Centers for Environmental Prediction (NCEP), European Centre for Medium-Range Weather Forecasts Interim Re-Analysis (ERA-Interim), Japanese 25-year Reanalysis (JRA25), and so on. However, the surface heat flux values in the TP from these reanalysis datasets differ from each other in magnitude and even in the spatial distribution pattern (Zhu *et al.*, 2012). This gives us an excuse to question the General Circulation Model (GCM) numerical simulation result in Boos and Kuang (2010). With the aid of high spatial resolution remote sensing land surface data, we now have the opportunity to investigate the spatiotemporal characteristics of the TPs land surface heat flux values. This method provides us another way to look at the TPs land–air interaction, as the satellite data can directly observe the TPs land surface thermal status.

The bulk transfer coefficient method is typically used to calculate the land surface sensible heat flux. Using China Meteorological Administration (CMA) weather station data, with different heat transfer coefficients, many researchers have pointed out the decelerating trends evident in the sensible heat flux on the TP, but these have decreased with different magnitudes (Duan and Wu, 2008; Yang *et al.*, 2011a). Unfortunately, station-based results are inadequate for determining the spatial pattern of the sensible heat flux for the entire TP due to the imbalanced distribution of CMA weather stations (these being mainly located in the central and eastern parts of the TP; there is consequently very little data available with cover the western TP). This makes previous land surface flux trend analysis problematic in representing the status of the whole TP. Remote sensing can provide us with a full coverage of the TP. Thus, using a combination of remote sensing data, reanalysis data, and *in situ* observations, scientists have attempted to estimate land surface heat fluxes, within the framework of the surface layer similarity theory, for the whole TP (Ma *et al.*, 2011; Chen *et al.*, 2014). However, previous studies such as these did not take into account the impact of any topographical differences when calculating sensible heat flux on the TP, even in its more mountainous areas (Amatya *et al.*, 2015).

In our study, we used an effective roughness length to calculate the sensible heat flux. This included the form drag caused by subgrid-scale orography (Han *et al.*, 2015), which makes the method to be more reasonable for the TP region. Then, monthly land surface heat flux values from 2001 to 2012 (i.e. for net radiation flux, sensible heat flux, latent heat flux, and ground heat flux) were estimated, using revised Surface Energy Balance System (SEBS) model (Su, 2002; Chen *et al.*, 2013b). Any trends in these flux values for the TP were analysed by reanalysing-meteorological and remote sensing data.

2. Model description and input data

In our study, land surface heat flux values were derived using the SEBS model (Su, 2002). The inputs included monthly meteorological data and remote sensing data. The meteorological dataset was developed at the Institute of Tibetan Plateau Research, Chinese Academy of Sciences (hereafter termed the 'ITPCAS meteorological forcing dataset') (Chen *et al.*, 2011). The ITPCAS meteorological forcing dataset covers the whole landmass of China and has the highest spatiotemporal resolution of any of the reanalysis data used. This dataset benefits in particular from the merging of the observations from 740 operational weather stations operated by CMA, and from its use of the Global Energy and Water Cycle Experiment – Surface Radiation Budget (GEWEX-SRB) shortwave radiation dataset (Pinker and Laszlo, 1992), the latter not having been used in any other forcing dataset. The details of the input datasets are shown in Table 1. In order to make the inputs spatially continuous, all the datasets were interpolated at a spatial resolution of $0.1° \times 0.1°$ (the resolution of the ITPCAS meteorological forcing dataset). The justification has been discussed in Chen *et al.* (2014). The relative short period of time for trend analysis (2001–2012) was due to the limits of the input data, as the remote sensing data starts from 2001 and ITPCAS meteorological forcing dataset ends in 2012. The model is described in detail below.

The land surface energy balance equation was written as:

$$R_{\mathrm{n}} = H + \mathrm{LE} + G_0 \tag{1}$$

where R_{n} is the net radiation flux, H is the sensible heat flux, LE is the latent heat flux, and G_0 is the ground heat flux, which is estimated by its relation with R_{n}. LE was computed using the evaporative fraction after deriving the other three variables in Equation (1), whilst considering dry and wet limits. Details can be found in Su (2002) and Chen *et al.* (2013a).

The net radiation flux was derived from:

$$R_{\mathrm{n}} = (1 - \alpha) \times \mathrm{SWD} + \mathrm{LWD} - \varepsilon \times \sigma \times T_s^4 \tag{2}$$

where α is the surface albedo obtained from the GlobAlbedo data (Muller *et al.*, 2011). The albedo values for 2012 were obtained by averaging the albedo values from preceding years, due to unavailability of data after 2011. Downward shortwave radiation (SWD) and downward longwave radiation (LWD) values were taken from the ITPCAS meteorological forcing dataset. Land surface

Table 1. Input datasets used in this study.

Variables	Data source	Availability	Temporal resolution	Spatial resolution
Downward shortwave	ITPCAS	1979–2012	3 h	0.1°
Downward longwave	ITPCAS	1979–2012	3 h	0.1°
Air temperature	ITPCAS	1979–2012	3 h	0.1°
Specific humidity	ITPCAS	1979–2012	3 h	0.1°
Wind speed	ITPCAS	1979–2012	3 h	0.1°
Land surface temperature	MOD11C3	2000 to now	1 month	0.05°
Land surface emissivity	MOD11C3	2000 to now	1 month	0.05°
Height of canopy	GLAS & SPOT VEGETATION	2000 to now	1 month	0.01°
Albedo	GlobAlbedo	1998–2011	1 month	0.05°
NDVI	SPOT VEGETATION	1998 to now	10 days	0.01°
DEM	ASTER GDEM	–	–	30 m

temperature (T_s) and emissivity (ε) values were derived using Moderate Resolution Imaging Spectroradiometer (MODIS) products.

For water surface (NDVI < 0 and albedo < 0.47), we used an equation of $G_0 = 0.5R_n$ (Gao *et al.*, 2011; Chen *et al.*, 2013a). For glacier area, G_0 is negligible according to Yang et al. (2011c) and we used an equation of $G_0 = 0.05R_n$. For canopy coverage area, the following equation was adopted (Su, 2002):

$$G_0 = R_n \times \left(r_c \times f_c + r_s \times \left(1 - f_c\right)\right) \tag{3}$$

where r_s and r_c are the ratios between ground heat flux and net radiation for bare soils and surfaces with fully covered vegetation, respectively, and f_c is the fractional vegetation cover.

The sensible heat flux was computed using the Monin–Obukhov similarity theory by solving the following three equations (Stull, 1988):

$$U = \frac{u_*}{\kappa}\left[\ln\left(\frac{z-d_0}{z_{0m}^{\text{eff}}}\right) - \psi_m\left(\frac{z-d_0}{L}\right) + \psi_m\left(\frac{z_{0m}^{\text{eff}}}{L}\right)\right] \tag{4a}$$

$$\theta_0 - \theta_a = \frac{H}{\kappa u_* \rho C_p}\left[\ln\left(\frac{z-d_0}{z_{0h}^{\text{eff}}}\right) - \psi_h\left(\frac{z-d_0}{L}\right) + \psi_h\left(\frac{z_{0h}^{\text{eff}}}{L}\right)\right] \tag{4b}$$

$$L = \frac{\rho C_p u_*^3 \theta_v}{\kappa g H} \tag{4c}$$

where U is the horizontal wind speed at height z, u_* is the friction velocity, κ is the von Kármán's constant, d_0 is the zero-plane displacement height, θ_0 and θ_a are the potential temperature at land surface and height z respectively, θ_v is the potential virtual temperature at height z, ρ is the density of air, C_p is the specific heat for moist air, g is the acceleration due to gravity, ψ_m and ψ_h are the stability correction functions for momentum and sensible heat transfer, respectively, and L is the Monin–Obukhov length.

The effective roughness lengths for momentum (z_{0m}^{eff}) and sensible heat (z_{0h}^{eff}) transfer were calculated as follows (Grant and Mason, 1990; Han *et al.*, 2015):

$$\ln^2\left(h/2z_{0m}^{\text{eff}}\right) = \frac{\kappa^2}{0.5D\lambda + \kappa^2/\ln^2\left(h/2z_{0m}\right)} \tag{5a}$$

$$\ln\left(h/2z_{0h}^{\text{eff}} + 1\right) = \ln\left(h/2z_{0h} + 1\right)\frac{\ln\left(h/2z_{0m} + 1\right)}{\ln\left(h/z_{0m}^{\text{eff}} + 1\right)} \tag{5b}$$

where z_{0m} and z_{0h} are the local scale roughness values for momentum and heat transfer, D is the form drag coefficient, and λ is the average density of the subgrid-scale roughness obstacles derived using digital elevation models (Han *et al.*, 2015). $D = 0.4$ was used in this work according to the investigation by Han *et al.* (2015).

The density of roughness obstacle is one of the most important parameters used to characterize the roughness of each grid (here with a size of $0.1° \times 0.1°$) land surface. λ can be calculated from A/S, where A is the average silhouette area of the roughness obstacles, i.e. the area transverse to the wind direction, and S is the horizontal area taken up by any large-scale obstacles. For two-dimensional obstacles, the estimation of A/S can be simplified to $A/S = h/l$, where h is the mean height of any obstacles, which in turn is assumed to be twice the standard deviation of the detrended elevation, and l is the average wavelength, which is assumed to be the mean distance between the tops of any obstacles. In this study, we took $h = 10$ m as a critical threshold to set the boundary for differentiating the effects of topography from any ground surface inhomogeneity. The geometric features of large-scale obstacles ($h > 10$ m) were used to calculate the topographical drag effect. These parameters were derived using Advanced Spaceborne Thermal Emission and Reflection Radiometer (ASTER) GDEM (ASTER Global DEM) Version 2 dataset (http://gdem.ersdac.jspacesystems.or.jp/index.jsp).

The difference between z_{0m}^{eff} and z_{0m} is that z_{0m} represents the shear stress caused by small-scale features, such as grass and trees, but z_{0m}^{eff} not only considers shear stress but also takes into account any form drag exerted by subgrid-scale topographical features. The details of the calculations of z_{0m} and z_{0h} can be found in Su (2002). A revised scheme for z_{0h} in Chen *et al.* (2013b) was adopted here as which has a better performance than original model for the TP.

3. Results and discussion

The accuracy of the model's input dataset and output land surface heat flux values should be evaluated before further analysis. In our study, the model inputs and remotely sensed land surface heat flux values were validated with *in situ* observations recorded at Qomolangma Station for Atmospheric Environmental Observation and Research, Chinese Academy of Sciences (hereafter termed the 'QOMS station'), and the Nam Co Monitoring and Research Station for Multisphere Interactions, Chinese Academy of Sciences (hereafter called the 'Namco station'), both on the TP. The QOMS station is located at 28.26°N, 86.95°E in a valley approximately 40 km north-west of Mt. Everest, at an altitude of 4276 m above sea level (asl). The land surface cover is mainly sandy soil with spare and short grass, and small rocks. The Namco station is located at 30.78°N, 90.96°E, on the southeastern shores of Nam Co Lake and on the northern slopes of the Nyainqentanglha Mountains, at an altitude of 4730 m asl. Alpine meadow and steppe grassland are widely distributed around the station. The instrumental setup at each station consists of: an eddy covariance system (Campbell CSAT3 3-D sonic anemometer, LI-COR LI-7500 infrared gas analyser) mounted at a height of 3.25 m at QOMS station, and 3.06 m at Namco station; a four-component radiation budget system (Kipp & Zonen, CNR-1) mounted at the height of 1.5 m; an atmosphere boundary layer (ABL) tower (Vaisala, Milos520), with which air temperature, relative humidity and wind speed are measured at 1.5, 2.0, 4.0, 10.0, and 20.0 m; soil moisture and temperature sensors buried at depths of 0.05, 0.10, and 0.15 m, respectively; and a soil heat flux plate (Hukseflux, HFP01) buried at a depth of 0.1 m.

The eddy covariance data were processed using TK3 software (Mauder and Foken, 2015). The procedure included despiking, double rotation of 3-D wind speed, time lag corrections, frequency response corrections (Moore, 1986), and corrections for density fluctuations (Webb *et al.*, 1980). The ground heat flux at the surface was calculated by adding the measured flux at plate depth to energy stored in the layer above the heat flux plate (Han *et al.*, 2016). Then, half hourly data were converted to daily data, and finally, monthly *in situ* variables were obtained for validation.

3.1. Validation

The accuracies of the model input dataset and outputs were evaluated using mean bias (MB) and root-mean-square error (RMSE), defined as follows:

$$\mathrm{MB} = \frac{\sum_{i=1}^{N} \left(\mathrm{obs}_i - x_i\right)}{N} \tag{6}$$

$$\mathrm{RMSE} = \sqrt{\frac{\sum_{i=1}^{N} \left(\mathrm{obs}_i - x_i\right)^2}{N}} \tag{7}$$

where, obs_i is the measured value, x_i is the modelled value, and N is the number of samples.

Available measurements observed at QOMS and Namco stations from 2007 to 2012 were used to validate the SEBS model inputs and outputs. Due to technical limitations, there were some values missing for both the QOMS and Namco stations for this period.

3.1.1. Validation of inputs

The ITPCAS meteorological forcing dataset has already been widely validated and used in land surface and hydrological modelling studies in the TP and China, and has been recognized to be the best of the reanalysis datasets currently available (Chen *et al.*, 2011, 2014; Guo and Wang, 2013; Liu and Xie, 2013). However, further validation of the ITPCAS meteorological forcing dataset was deemed necessary. Apart from the meteorological variables, land surface parameters including land surface temperature, albedo and height of canopy are also crucial to any estimation of land surface heat flux values. A NDVI-based short canopy estimation and satellite sensed forest height developed in Chen *et al.* (2014) was used to represent canopy height information for the TP.

Temporal comparisons of land surface albedo and temperature values are shown in Figure 1. We found that the satellite-based albedo values were close to *in situ* observed land surface albedo values, with a MB of −0.01 at QOMS station, and 0.01 at Namco station, and with a RMSE of 0.02 and 0.03 at the QOMS and Namco stations, respectively. Land surface temperature values were also found to be close to *in situ* observations, with a MB of −0.6 K and −1.8 K at the QOMS and Namco stations, respectively, and with a RMSE of 2.8 K at both the QOMS and Namco stations. Further, the correlation coefficients (R) of land surface temperatures were both ≥ 0.9 at the two stations. These results all indicate that the remote sensing-based land surface albedo and temperature values are of good quality and are able to capture variations in *in situ* observed variables.

3.1.2. Validation of land surface heat flux values

The use of estimated land surface heat flux values for reanalysis without any validation against ground-based measurements is questionable (Meir and Woodward, 2010).

In this study, remote sensing-based land surface heat flux values were validated using *in situ* eddy covariance measurements from the QOMS and Namco stations. Figure 2 shows the comparison between observed and estimated land surface heat flux values. The estimated net radiation flux values were close to the observations made at both the QOMS and Namco stations, with low RMSE and MB values, and high R values. This appears to be due to the accurate input of SWD and LWD data from ITPCAS meteorological forcing dataset, and land surface albedo and land surface temperature values derived from remote sensing data. Han *et al.* (2016) pointed out that it is imperative to consider the effect of topography in mountainous areas

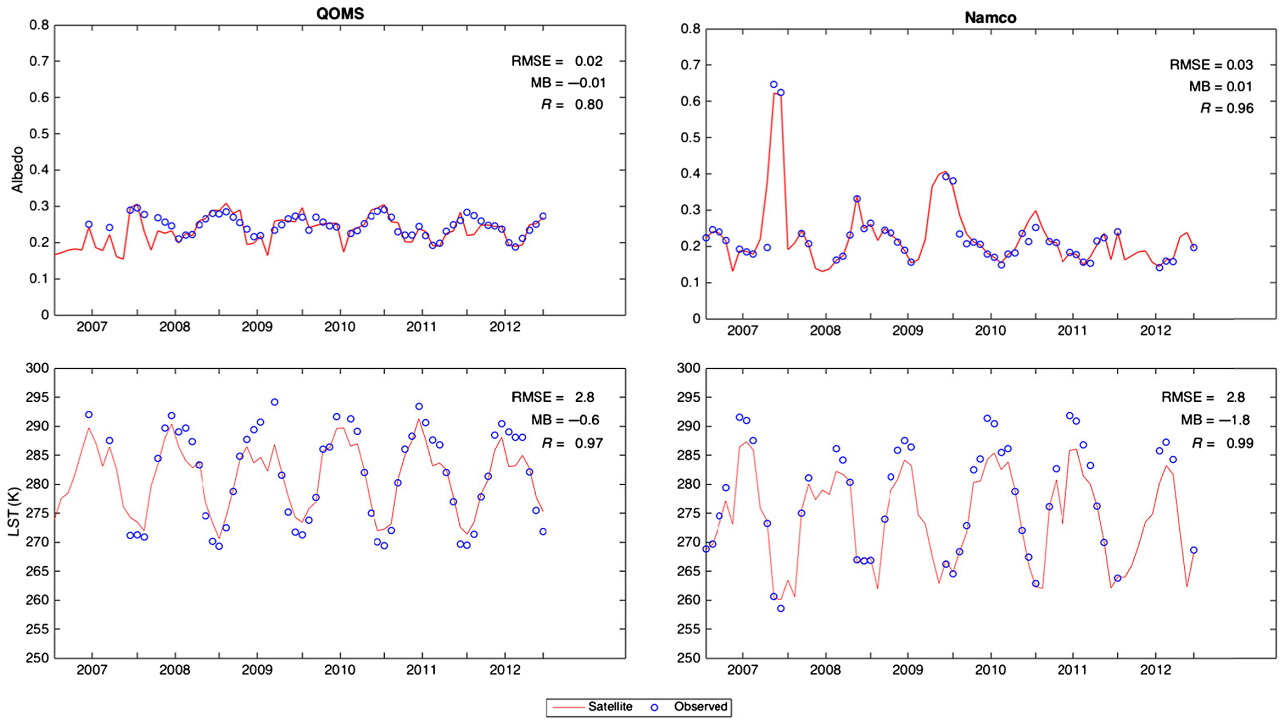

Figure 1. Comparison between observed and remote sensing-based land surface albedo and land surface temperature (LST) at the QOMS and Namco stations. RMSE is the root-mean-square error, MB is mean bias, and R is the correlation coefficient. [Colour figure can be viewed at wileyonlinelibrary.com].

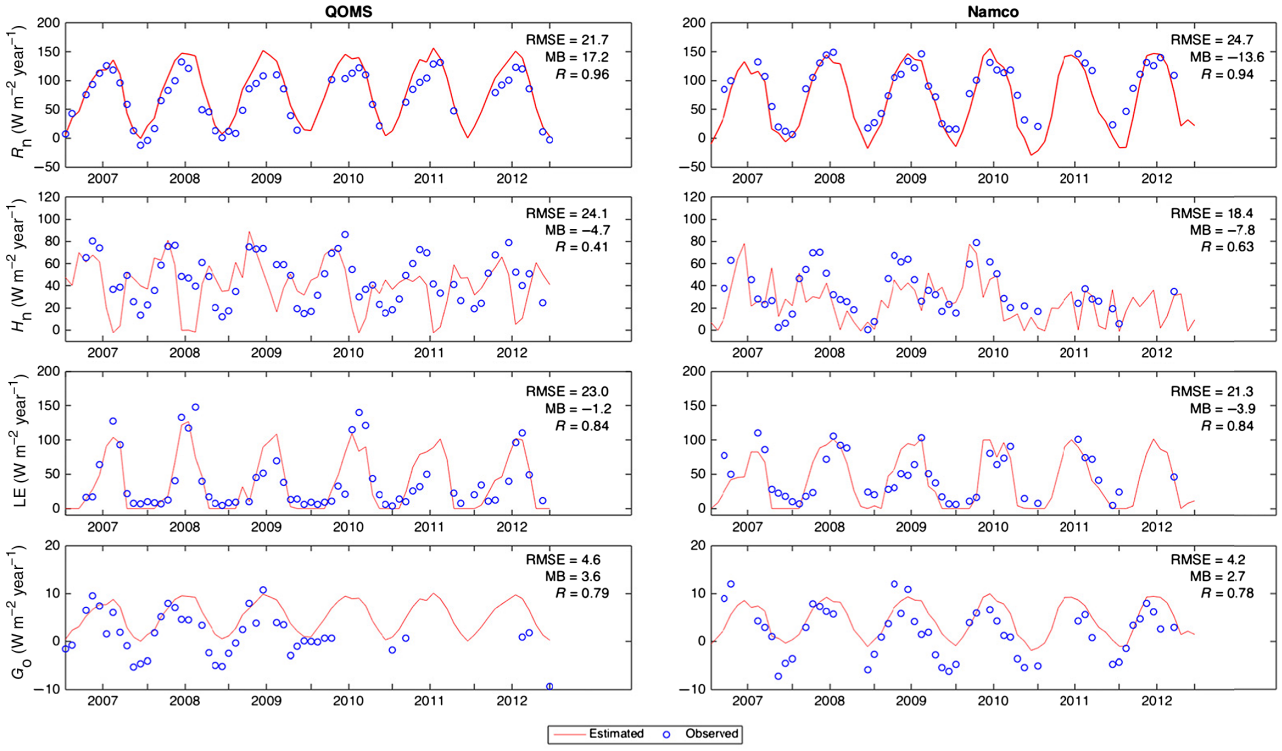

Figure 2. Comparison between observed and estimated land surface heat flux values at the QOMS and Namco stations. RMSE is root-mean-square error, MB is mean bias, and R is the correlation coefficient. [Colour figure can be viewed at wileyonlinelibrary.com].

of the TP when estimating SWD and land surface albedo. However, these factors were not considered in the SWD and land surface albedo input data, possibly causing the errors encountered.

The sensible heat flux was underestimated, with a MB of 4.7 W m^{-2} at QOMS station, and of 7.8 W m^{-2} at Namco station, and with a low R of 0.41 at QOMS station, and 0.63 at Namco station. Su (2002) pointed out that any error

in SEBS-estimated sensible heat flux values would most probably be related to the uncertainty in roughness length used in the heat transfer equation, in addition to temperature, wind speed, and stability correction. In our study, the model's wind speed input data derived from the ITP-CAS meteorological forcing dataset may not have been very accurate, due to the limited number of CMA weather stations on the TP (Yang *et al.*, 2011b). An energy imbalance existed at most of the studied sites, with a mean imbalance of the order of 20% (Wilson *et al.*, 2002); this is likely to have affected our validation considerably. Furthermore, the differences in measurement heights, differences in the fetch areas of *in situ* measurements, and in SEBS estimates, may also have contributed to the differences in the results. The RMSE values of latent heat flux were $\leq 23\ \mathrm{W\,m^{-2}}$ at both the validation stations. With lower relative RMSE and MB values, and higher R values at both of the two validation stations, the latent heat flux values were taken as more accurate than the sensible heat flux values in this study.

The RMSE values of land surface sensible and latent heat flux were no more than $25\ \mathrm{W\,m^{-2}}$ in this study, lower than the RMSE values produced using other statistical methods (Kalma *et al.*, 2008; Jiménez *et al.*, 2009; Vinukollu *et al.*, 2011). With a spatial resolution of $0.1^\circ \times 0.1^\circ$, the land surface heat flux values were therefore taken as suitable for spatial and trend analysis.

3.2. Spatial distribution of land surface heat flux values

Using the annual averaged land surface heat flux values from 2001 to 2012, we analysed the spatial patterns of heat fluxes on the TP. Figure 3 shows the average annual map of land surface heat flux values. The highest net radiation flux values (Figure 3(a)) were found in the southeastern Tibet and Hengduan Mountains. The lowest net radiation values were located along the northern margins of the TP, and high, snow- and ice-bound, mountainous areas with high-albedo values. Ground heat flux values (Figure 3(b)) followed a similar pattern, but compared with net radiation flux values, these values were either small or negligible. High sensible heat flux values (Figure 3(c)) were recorded for the western part of the TP, the northern slopes of the Himalaya, and the northeastern margins of the TP. Latent heat flux values (Figure 3(d))

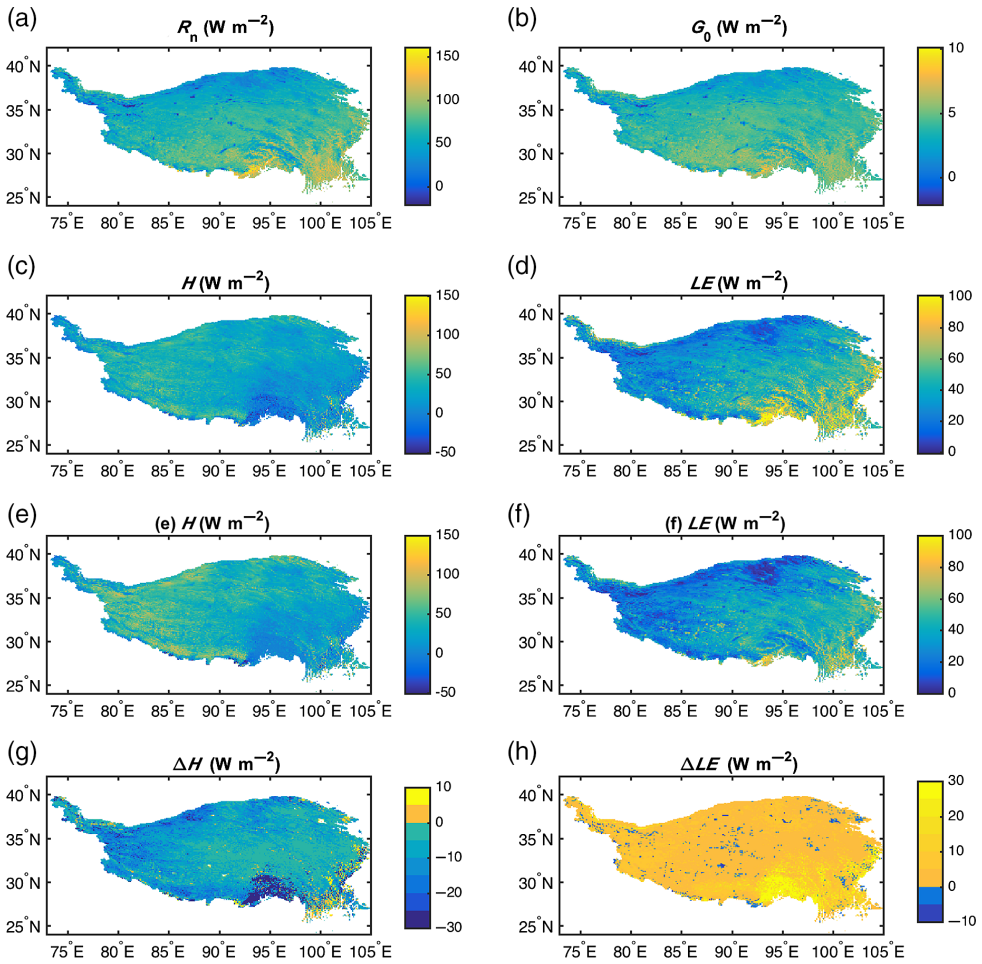

Figure 3. Average annual maps of land surface heat flux values on the TP from 2001 to 2012: (a) net radiation flux; (b) ground heat flux; (c) sensible heat flux after using effective roughness length; (d) latent heat flux after using effective roughness length; (e) sensible heat flux before using effective roughness length; and (f) latent heat flux before using effective roughness length. (g) The difference of sensible heat flux between with and without using effective roughness length (c–e) and (h) the difference of latent heat flux between with and without using effective roughness length (d–f). [Colour figure can be viewed at wileyonlinelibrary.com].

displayed a southeast-to-northwest decreasing gradient across the TP in line with the abundance value of rainfall transported across the region by the ASM (Ye and Gao, 1979). Areas along the eastern margins of the TP, the Hengduan Mountains, part of southeastern Tibet, and the Lhasa River Basin all exhibited high levels of latent heat flux. The northwestern margins of the TP, with many rives and oases supplied by glacial meltwater, also evinced high latent heat flux. Low latent heat flux values were recorded in the north and west of the TP, where dry and cold climatic conditions predominate.

In order to compare with and without the subgrid-scale topographical effect on the land surface heat flux values calculation, Figures 3(c)–(f) show land surface sensible heat flux and latent heat flux values as estimated by roughness length scheme with and without the improved roughness parameterization scheme in Section 2. And the differential maps for sensible heat flux and latent heat flux were also plotted in Figures 3(g) and (h), respectively. It was found that the big differences in sensible and latent heat flux values evident from the two schemes were mainly located in the rugged mountainous areas, such as the Hengduan Mountains area, the southeast of Tibet, the northwestern margins of the TP, ans so on. After the introduction of effective aerodynamic roughness parameters, land surface sensible heat flux became weaker, especially in area with complex topographical environments. We suggested that this is likely to be principally because wind speed decreases to adapt to a rugged terrain. According to the energy balance theory, sensible heat flux values should decrease, and latent heat flux values increase. This would also explain why latent heat flux values become larger after including the influence of a subgrid-scale topography in areas such as Hengduan Mountains, southeastern Tibet, and the northwestern margins of the TP.

3.3. Analysis of trends

Linear trend analysis was used to analyse the regional trends in land surface heat flux values. A linear model was used to simulate the land surface heat flux variable (Y_t) against time (t) (Yao *et al.*, 2013), thus:

$$Y_t = Y_0 + bt + \varepsilon_t \tag{8}$$

where Y_0 is the y-intercept, b is the slope, and ε_t is the error term.

The significance tests for derived tendencies were calculated using Student's t-test, with a $n-2$ degree of freedom (Pinker *et al.*, 2005), thus:

$$t_{xy} = r_{xy}\sqrt{\frac{n-2}{1-r_{xy}^2}} \tag{9}$$

where r_{xy} is the correlation coefficient between the original time series and the linear fitted time series, and n is the number of samples.

We then analysed the linear trends and significance test maps of land surface heat flux values on the TP from 2001 to 2012 (Figure 4). The significance test was done using Student's t-test with $n-2$ degree of freedom.

Net radiation flux values, in general, showed a slight increase across the whole TP. This increasing trend was clearest in high, mountainous areas and in the central TP. Net radiation flux values over the mountain ranges of the Kunlun, Qilian, Karakoram, Himalaya, and Hengduan mountains have increased over the past 12 years, perhaps caused by the glacial retreat also seen in these areas (Scherler *et al.*, 2011; Yao *et al.*, 2012a). van der Velde *et al.* (2014) pointed out that soil moisture content has increased across the central TP from 1987 to 2008. Glacial retreat and topsoil wetting will inevitably cause decrease in land surface albedo values, and a greater absorption of solar radiation, with a consequent increase in net radiation flux values. Ground heat flux values in our study were derived from their linear relation with net radiation flux values. It is therefore perhaps unsurprising that the former showed a similar spatial trend to the latter.

Sensible heat flux values showed significant decreases across most parts of the TP. The average decrease trend in sensible heat flux for the whole TP changed from $-6.8\,\mathrm{W\,m^{-2}}$ per decade to $-5.3\,\mathrm{W\,m^{-2}}$ per decade after taking into account the influence of subgrid-scale topography. The weakening trend in surface sensible heat flux values discovered by our study was two times that reported by Duan and Wu (2008) and Yang *et al.* (2011a). Apart from the contribution by subgrid-scale topography influence, this may well be because our estimates included much more information from western TP, where sensible heat flux values have weakened significantly (Figure 4). Differences in the time periods considered might be another reason. In general, sensible heat flux increases with an increase in wind speed and any ground-air temperature difference. Figure 5 shows the spatial trends and significance test maps of wind speed and ground-air temperature differences for the study region. The decreases in sensible heat flux values noted for the northern TP can perhaps be explained by the combined effect of a decrease in wind speeds as well as differences in ground-air temperatures. However, for almost all the YZR basin, land surface sensible heat flux values have increased over the past 12 years. It would seem that this increase in sensible heat flux values in the YZR Basin is principally a reflection of increases in the ground-air temperature difference. The increase in sensible heat flux values in the southeastern Tibet could also potentially be largely attributed to increase in ground-air temperature difference in this area. Latent heat flux values increased for the whole TP, apart from in the YZR Basin. Guo and Wang (2013) pointed out that the TPs near-surface permafrost layer has degenerated as a response to regional climatic warming from 1981 to 2010. The increased net radiation flux and soil moisture content, and degradation of permafrost-frozen soil, could therefore be reasonably assumed to be responsible for the increases seen in latent heat flux values. Furthermore, the increased level of precipitation in the central-eastern TP (Yang *et al.*, 2014) and vegetation greening (Shen *et al.*, 2015) could also explain the raising trend seen in latent heat flux values on the TP. Li *et al.* (2015) reported that precipitation decreased year on year from 1999 to 2013,

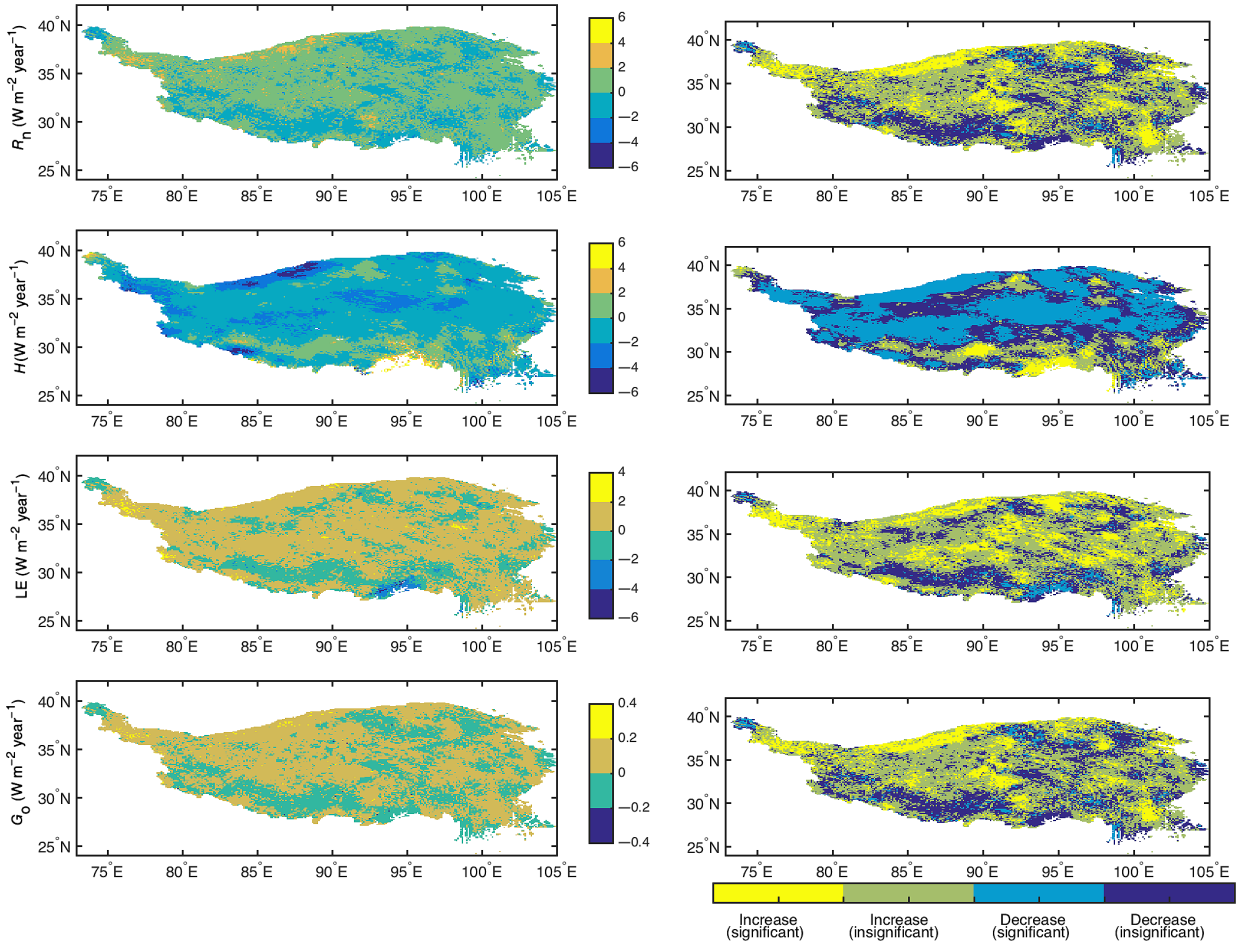

Figure 4. Linear trends (left column) and significance test (right column) maps of net radiation flux (R_n), sensible heat flux (H), latent heat flux (LE), and ground heat flux (G_0) on the TP from 2001 to 2012, with the unit used in trend analysis being W m^{-2} year^{-1}. The trends were classified into four categories according to statistical linear trend analysis: a significant increase ($p < 0.1$); a significant decrease ($p < 0.1$); an insignificant increase ($p > 0.1$); and an insignificant decrease ($p > 0.1$). [Colour figure can be viewed at wileyonlinelibrary.com].

which could explain why latent heat flux values have weakened in the YZR Basin.

Although the average trend in surface sensible heat flux values have been characterized by a general weakening across the TP, some areas have exhibited increases in value. Trends in surface sensible heat flux values and other surface heat flux values also show dramatically different characteristics in different areas of the TP. This highlights the need to use high-resolution datasets to estimate land surface heat flux values on the TP. And furthermore, the seasonal variations and trends in land surface heat flux values are also remarkable on the TP. The seasonal dependence of land surface heat flux values would be more complicated as the nonuniform seasonal changes in the land surface and atmospheric variables on the TP (Yang *et al.*, 2014). It would be significant and interesting to investigate the characteristics and drivers of seasonal variations and dependences of land surface heat flux values in future studies.

4. Summary and conclusion

Over the past several decades, the TP has experienced rapid climatic warming, which has affected its energy and water cycles. As one of the major drivers of these energy and water cycles, the land surface energy budget and the manner in which it has changed must receive renewed focus in any future land–atmosphere interaction studies. In our study, monthly land surface heat flux values over the TP from 2001 to 2012 were estimated at a resolution of 0.1° using a revised SEBS model, combined with various remote sensing products and the ITPCAS meteorological forcing dataset as input. In order to parameterize the effect of the region's topography on turbulent heat flux values, a scheme of effective roughness including the influences of both subgrid-scale topography roughness and canopy roughness was introduced into the SEBS model. The estimated land surface heat flux values were then validated using *in situ* observations at the QOMS and Namco stations on the TP. Annual trends in these data were then analysed.

The remote sensing-based land surface heat flux values were estimated at a spatial resolution of ~10 km. This is in contrast to the footprint of eddy covariance observations, which ranged from tens to hundreds of metres. This mismatch in spatial representation between estimated fluxes and *in situ* observations will most likely

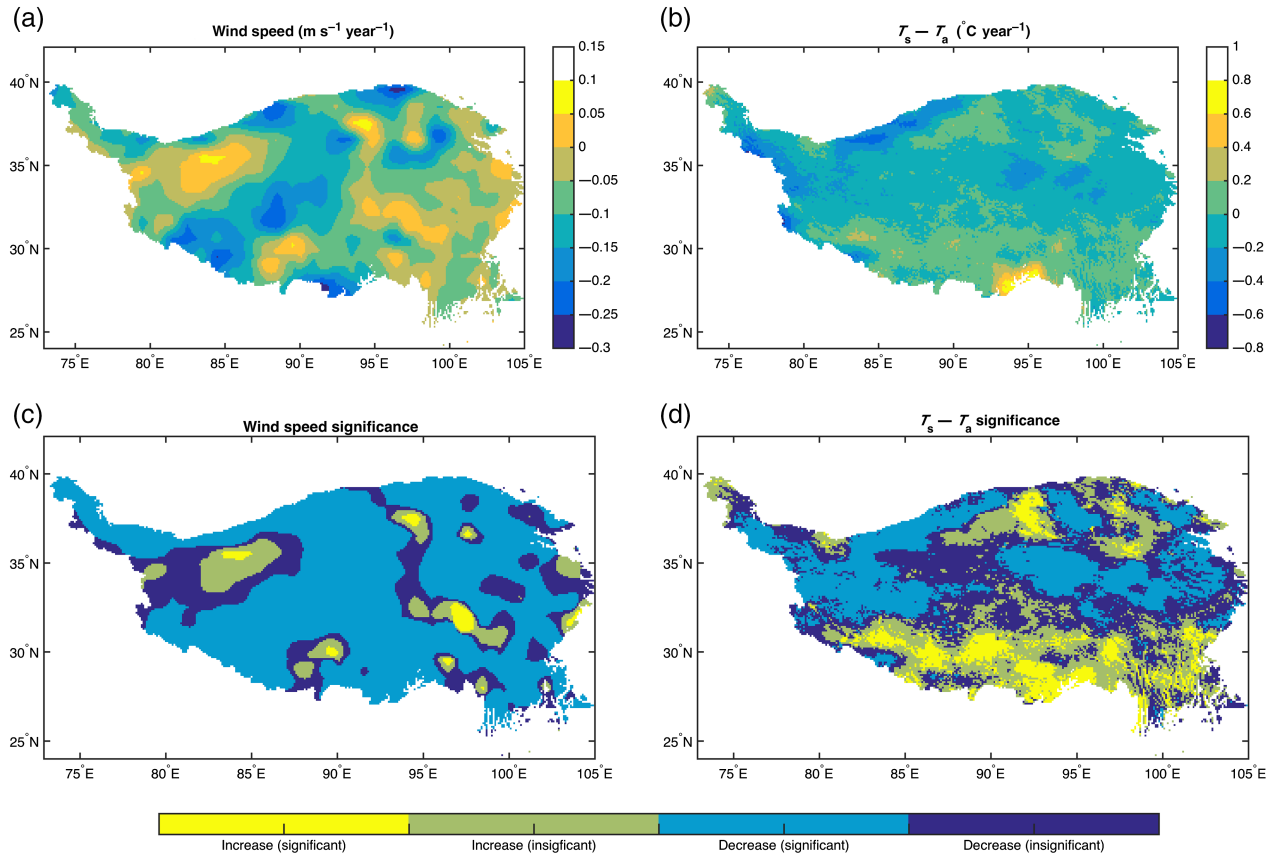

Figure 5. Trend and significance test maps of wind speed (left column) and ground-air temperature difference (right column) on the TP from 2001 to 2012. The trends were classified into four categories according to statistical linear trend analysis: a significant increase ($p < 0.1$); a significant decrease ($p < 0.1$); an insignificant increase ($p > 0.1$); and an insignificant decrease ($p > 0.1$). [Colour figure can be viewed at wileyonlinelibrary .com].

have resulted in errors during the validation process. However, the estimated surface heat flux values are nonetheless able to capture seasonal and annual variations, and can then reasonably be used for trend analysis. It was found that the TP has experienced an overall slight increase in land surface net radiation flux values, while sensible heat flux values have decreased and latent heat flux values have increased year on year from 2001 to 2012 in the context of climate change. However, the changing trends in different regions appear dramatically different. Areas which have experienced increased net radiation flux values are located in high, mountainous areas and the central TP. This finding might relate to changes in the condition of particular land surfaces in these areas. In contrast to other regions on the TP, sensible heat flux values increased, and latent heat flux values decreased, in the YZR Basin area. This could be explained by increases in the ground-air temperature difference and falling levels of precipitation in this area. Latent heat flux values have been increased over almost the entire TP, except for in the YZR Basin. High spatial resolution remote sensing data and reanalysis meteorological data give us a unique opportunity to derive and analyse spatial patterns and trend in the spatiotemporal distribution of surface heat flux values on the data-sparse TP, and especially in its western sector.

Estimating regional land surface heat flux values is not an easy job, especially on the TP, which is notorious for its lack of meteorological and climatic observations, and for its complex topography. This highlights the importance of *in situ* observations and the application of remote sensing data. In particular, the development of reliable parameterization schemes may effectively reduce possible uncertainties in land-atmosphere studies.

Acknowledgements

This study was funded by the National Natural Science Foundation of China (grant nos. 91337212, 41661144043, and 41522501), the Chinese Academy of Sciences (grant no. XDB03030201), the International Partnership Program of the Chinese Academy of Sciences (grant no. 131C11KYSB20160061), the CMA Special Fund for Scientific Research in the Public Interest (grant no GYHY201406001), and the EU-FP7 'CORE-CLIMAX' Project (grant no. 313085). The ITPCAS meteorological forcing dataset used in this study was developed by the Data Assimilation and Modeling Center for Tibetan Multi-spheres, Institute of Tibetan Plateau Research, Chinese Academy of Sciences. MODIS data were obtained from the NASA Land Processes Distributed Active Archive Center (https://lpdaac.usgs.gov/). Global 1 km

canopy height data were obtained from the Oak Ridge National Laboratory Distributed Active Archive Center for Biogeochemical Dynamics (http://webmap.ornl.gov/wcsdown/wcsdown.jsp?dg_id=10023_1). NDVI data was supplied by the Systeme pour l'Observation de la Terre (SPOT) VEGETATION sensor, as distributed by Vito (http://free.vgt.vito.be/). The authors should like to thank all colleagues working at the QOMS and Namco stations for their maintenance of the instruments.

References

Amatya PM, Ma Y, Han C, Wang B, Devkota LP. 2015. Recent trends (2003–2013) of land surface heat fluxes on the southern side of the central Himalayas, Nepal. *J. Geophys. Res-Atmos.* **120**: 11,957–11,970. https://doi.org/10.1002/2015JD023510.

Boos WR, Kuang Z. 2010. Dominant control of the South Asian monsoon by orographic insulation versus plateau heating. *Nature* **463**: 218–222. https://doi.org/10.1038/nature08707.

Boos WR, Kuang Z. 2013. Sensitivity of the South Asian monsoon to elevated and non-elevated heating. *Sci. Rep.* **3**: 1192. https://doi.org/10.1038/srep01192.

Chen Y, Yang K, He J, Qin J, Shi J, Du J, He Q. 2011. Improving land surface temperature modeling for dry land of China. *J. Geophys. Res-Atmos.* **116**: D20104. https://doi.org/10.1029/2011JD015921.

Chen X, Su Z, Ma Y, Yang K, Wang B. 2013a. Estimation of surface energy fluxes under complex terrain of Mt. Qomolangma over the Tibetan Plateau. *Hydrol. Earth Syst. Sci.* **17**: 1607–1618. https://doi.org/10.5194/hess-17-1607-2013.

Chen X, Su Z, Ma Y, Yang K, Wen J, Zhang Y. 2013b. An improvement of roughness height parameterization of the surface energy balance system (SEBS) over the Tibetan Plateau. *J. Appl. Meteorol. Climatol.* **52**: 607–622. https://doi.org/10.1175/JAMC-D-12-056.1.

Chen X, Su Z, Ma Y, Liu S, Yu Q, Xu Z. 2014. Development of a 10-year (2001–2010) 0.1° data set of land-surface energy balance for mainland China. *Atmos. Chem. Phys.* **14**: 13097–13117. https://doi.org/10.5194/acp-14-13097-2014.

Duan A, Wu G. 2008. Weakening trend in the atmospheric heat source over the Tibetan Plateau during recent decades. Part I: observations. *J. Clim.* **21**: 3149–3164. https://doi.org/10.1175/2007JCLI1912.1.

Gao ZQ, Liu CS, Gao W, Chang NB. 2011. A coupled remote sensing and the Surface Energy Balance with Topography Algorithm (SEBTA) to estimate actual evapotranspiration over heterogeneous terrain. *Hydrol. Earth Syst. Sci.* **15**: 119–139. https://doi.org/10.5194/hess-15-119-2011.

Grant ALM, Mason PJ. 1990. Observations of boundary-layer structure over complex terrain. *Q. J. R. Meteorol. Soc.* **116**: 159–186. https://doi.org/10.1002/qj.49711649107.

Guo D, Wang H. 2013. Simulation of permafrost and seasonally frozen ground conditions on the Tibetan Plateau, 1981–2010. *J. Geophys. Res-Atmos.* **118**: 5216–5230. https://doi.org/10.1002/jgrd.50457.

Han C, Ma Y, Su Z, Chen X, Zhang L, Li M, Sun F. 2015. Estimates of effective aerodynamic roughness length over mountainous areas of the Tibetan Plateau. *Q. J. R. Meteorol. Soc.* **141**: 1457–1465. https://doi.org/10.1002/qj.2462.

Han C, Ma Y, Chen X, Su Z. 2016. Estimates of land surface heat fluxes of the Mt. Everest region over the Tibetan Plateau utilizing ASTER data. *Atmos. Res.* **168**: 180–190. https://doi.org/10.1016/j.atmosres.2015.09.012.

He B, Wu G, Liu Y, Bao Q. 2015. Astronomical and hydrological perspective of mountain impacts on the Asian Summer Monsoon. *Sci. Rep.* **5**: 17586. https://doi.org/10.1038/srep17586.

Jiménez C, Prigent C, Aires F. 2009. Toward an estimation of global land surface heat fluxes from multisatellite observations. *J. Geophys. Res-Atmos.* **114**: D06305. https://doi.org/10.1029/2008JD011392.

Kalma J, McVicar T, McCabe M. 2008. Estimating land surface evaporation: a review of methods using remotely sensed surface temperature data. *Surv. Geophys.* **29**: 421–469. https://doi.org/10.1007/s10712-008-9037-z.

Li H, Li Y, Shen W, Li Y, Lin J, Lu X, Xu X, Jiang J. 2015. Elevation-dependent vegetation greening of the Yarlung Zangbo River Basin in the Southern Tibetan Plateau, 1999–2013. *Remote Sens.* **7**: 15844.

Liu JG, Xie ZH. 2013. Improving simulation of soil moisture in China using a multiple meteorological forcing ensemble approach. *Hydrol. Earth Syst. Sci.* **17**: 3355–3369. https://doi.org/10.5194/hess-17-3355-2013.

Ma Y, Kang S, Zhu L, Xu B, Tian L, Yao T. 2008. Roof of the world: Tibetan observation and research platform. *Bull. Am. Meteorol. Soc.* **89**: 1487–1492. https://doi.org/10.1175/2008BAMS2545.1.

Ma Y, Zhong L, Wang B, Ma W, Chen X, Li M. 2011. Determination of land surface heat fluxes over heterogeneous landscape of the Tibetan Plateau by using the MODIS and in situ data. *Atmos. Chem. Phys.* **11**: 10461–10469. https://doi.org/10.5194/acp-11-10461-2011.

Mauder M, Foken T. 2015. Eddy-covariance software TK3. Documentation and Instruction Manual of the Eddy-Covariance Software Package TK3 (update), University of Bayreuth, Bayreuth, Germany, pp. 67 (ISSN 1614-8916). https://doi.org/10.5281/zenodo.20349.

Meir P, Woodward FI. 2010. Amazonian rain forests and drought: response and vulnerability. *New Phytol.* **187**: 553–557. https://doi.org/10.1111/j.1469-8137.2010.03390.x.

Moore CJ. 1986. Frequency response corrections for eddy correlation systems. *Bound.-Layer Meteorol.* **37**: 17–35. https://doi.org/10.1007/bf00122754.

Muller J-P, Lewis P, Fischer J, North P, Framer U. 2011. The ESA GlobAlbedo Project for mapping the Earth's land surface albedo for 15 years from European sensors, paper presented at the European Geophysical Union conference. *Geophys. Res. Abstr.* **13**: EGU2011–EGU10969.

Pinker RT, Laszlo I. 1992. Modeling surface solar irradiance for satellite applications on a global scale. *J. Appl. Meteorol.* **31**: 194–211. https://doi.org/10.1175/1520-0450(1992)031<0194:MSSIFS>2.0.CO;2.

Pinker RT, Zhang B, Dutton EG. 2005. Do satellites detect trends in surface solar radiation? *Science* **308**: 850–854. https://doi.org/10.1126/science.1103159.

Scherler D, Bookhagen B, Strecker MR. 2011. Spatially variable response of Himalayan glaciers to climate change affected by debris cover. *Nat. Geosci.* **4**: 156–159. https://doi.org/10.1038/ngeo1068.

Shen M, Piao S, Jeong S-J, Zhou L, Zeng Z, Ciais P, Chen D, Huang M, Jin C-S, Li LZX, Li Y, Myneni RB, Yang K, Zhang G, Zhang Y, Yao T. 2015. Evaporative cooling over the Tibetan Plateau induced by vegetation growth. *Proc. Natl. Acad. Sci.* **112**: 9299–9304. https://doi.org/10.1073/pnas.1504418112.

Stull RB. 1988. *An Introduction to Boundary Layer Meteorology*. Kluwer Academic Publishers: Dordrecht.

Su Z. 2002. The surface energy balance system (SEBS) for estimation of turbulent heat fluxes. *Hydrol. Earth Syst. Sci.* **6**: 85–100. https://doi.org/10.5194/hess-6-85-2002.

van der Velde R, Salama MS, Pellarin T, Ofwono M, Ma Y, Su Z. 2014. Long term soil moisture mapping over the Tibetan Plateau using Special Sensor Microwave/Imager. *Hydrol. Earth Syst. Sci.* **18**: 1323–1337. https://doi.org/10.5194/hess-18-1323-2014.

Vinukollu RK, Wood EF, Ferguson CR, Fisher JB. 2011. Global estimates of evapotranspiration for climate studies using multi-sensor remote sensing data: evaluation of three process-based approaches. *Remote Sens. Environ.* **115**: 801–823. https://doi.org/10.1016/j.rse.2010.11.006.

Webb EK, Pearman GI, Leuning R. 1980. Correction of flux measurements for density effects due to heat and water vapour transfer. *Q. J. R. Meteorol. Soc.* **106**: 85–100. https://doi.org/10.1002/qj.49710644707.

Wilson K, Goldstein A, Falge E, Aubinet M, Baldocchi D, Berbigier P, Bernhofer C, Ceulemans R, Dolman H, Field C, Grelle A, Ibrom A, Law BE, Kowalski A, Meyers T, Moncrieff J, Monson R, Oechel W, Tenhunen J, Valentini R, Verma S. 2002. Energy balance closure at FLUXNET sites. *Agric. For. Meteorol.* **113**: 223–243. https://doi.org/10.1016/S0168-1923(02)00109-0.

Wu G, Liu Y, He B, Bao Q, Duan A, Jin F-F. 2012. Thermal controls on the Asian summer monsoon. *Sci. Rep.* **2**: 404. https://doi.org/10.1038/srep00404.

Wu G, Duan A, Liu Y, Mao J, Ren R, Bao Q, He B, Liu B, Hu W. 2015. Tibetan Plateau climate dynamics: recent research progress and outlook. *Natl. Sci. Rev.* **2**: 100–116. https://doi.org/10.1093/nsr/nwu045.

Yanai M, Wu G. 2006. Effects of the Tibetan Plateau. In *The Asian Monsoon*, Wang B (ed). Springer Berlin: Heidelberg, Germany, 513–549.

Yang K, Guo X, Wu B. 2011a. Recent trends in surface sensible heat flux on the Tibetan Plateau. *Sci. China Earth Sci.* **54**: 19–28. https://doi.org/10.1007/s11430-010-4036-6.

Yang K, Guo X, He J, Qin J, Koike T. 2011b. On the climatology and trend of the atmospheric heat source over the Tibetan Plateau: an experiments-supported revisit. *J. Clim.* **24**: 1525–1541. https://doi.org/10.1175/2010JCLI3848.1.

Yang W, Guo X, Yao T, Yang K, Zhao L, Li S, Zhu M. 2011c. Summertime surface energy budget and ablation modeling in the ablation zone of a maritime Tibetan glacier. *Journal of Geophysical Research: Atmospheres*. **116**: D14116. https://doi.org/10.1029/2010JD015183.

Yang K, Ding B, Qin J, Tang W, Lu N, Lin C. 2012. Can aerosol loading explain the solar dimming over the Tibetan Plateau? *Geophys. Res. Lett.* **39**: L20710. https://doi.org/10.1029/2012GL053733.

Yang K, Wu H, Qin J, Lin C, Tang W, Chen Y. 2014. Recent climate changes over the Tibetan Plateau and their impacts on energy and water cycle: a review. *Glob. Planet. Change* **112**: 79–91. https://doi.org/10.1016/j.gloplacha.2013.12.001.

Yao T, Thompson L, Yang W, Yu W, Gao Y, Guo X, Yang X, Duan K, Zhao H, Xu B, Pu J, Lu A, Xiang Y, Kattel DB, Joswiak D. 2012a. Different glacier status with atmospheric circulations in Tibetan Plateau and surroundings. *Nat. Clim. Change* **2**: 663–667. https://doi.org/10.1038/nclimate1580.

Yao T, Thompson LG, Mosbrugger V, Zhang F, Ma Y, Luo T, Xu B, Yang X, Joswiak DR, Wang W, Joswiak ME, Devkota LP, Tayal S, Jilani R, Fayziev R. 2012b. Third pole environment (TPE). *Environ. Dev.* **3**: 52–64. https://doi.org/10.1016/j.envdev.2012.04.002.

Yao Y, Liang S, Cheng J, Liu S, Fisher JB, Zhang X, Jia K, Zhao X, Qin Q, Zhao B, Han S, Zhou G, Zhou G, Li Y, Zhao S. 2013. MODIS-driven estimation of terrestrial latent heat flux in China based on a modified Priestley–Taylor algorithm. *Agric. For. Meteorol.* **171–172**: 187–202. https://doi.org/10.1016/j.agrformet.2012.11.016.

Ye D, Gao Y. 1979. *The Meteorology of the Qinghai-Xizang (Tibet) Plateau (in Chinese)*. Science Press: Beijing, 278 pp.

Zhu X, Liu Y, Wu G. 2012. An assessment of summer sensible heat flux on the Tibetan Plateau from eight data sets. *Sci. China Earth Sci.* **55**: 779–786. https://doi.org/10.1007/s11430-012-4379-2.

